PERGAMON

International Journal of Heat and Mass Transfer 46 (2003) 771–780

International Journal of HEAT and MASS TRANSFER

www.elsevier.com/locate/ijhmt

Calculation of turbulent flow and heat transfer in a porous-baffled channel

Yue-Tzu Yang *, Chih-Zong Hwang

Department of Mechanical Engineering, National Cheng Kung University, Tainan 701, Taiwan, ROC

Received 24 August 2001; received in revised form 28 August 2002

Abstract

This study presents the numerical predictions on the turbulent fluid flow and heat transfer characteristics for rectangular channel with porous baffles which are arranged on the bottom and top channel walls in a periodically staggered way. The turbulent governing equations are solved by a control volume-based finite difference method with power-law scheme and the k–ε turbulence model associated with wall function to describe the turbulent structure. The velocity and pressure terms of momentum equations are solved by SIMPLE (semi-implicit method for pressure-linked equation) method.

The parameters studied include the entrance Reynolds number Re (1×10^4–5×10^4), the baffle height ($h = 10$, 20 and 30 mm) and kind of baffles (solid and porous); whereas the baffle spacing S/H are fixed at 1.0 and the working medium is air. The numerical calculations of the flow field indicate that the flow patterns around the porous- and solid-type baffles are entirely different due to different transport phenomena and it significantly influences the local heat transfer coefficient distributions. Relative to the solid-type baffle channel, the porous-type baffle channel has a lower friction factor due to less channel blockage.

Concerning the heat transfer effect, both the solid-type and porous-type baffles walls enhanced the heat transfer relative to the smooth channel. It is further found that at the higher baffle height, the level of heat transfer augmentation is nearly the same for the porous-type baffle, the only difference being the Reynolds number dependence. As expected, the centerline-averaged Nusselt number ratio increases with increasing the baffle height because of the flow acceleration.

1. Introduction

The flow separation in ducts with segmented baffles has many engineering applications, e.g. shell-and-tube heat exchangers with segmented baffles, air-cooled solar collectors, and internally cooled turbine blades. Augmentation techniques usually employ baffles attached to the heated surface so as to provide an additional heat transfer surface area and to promote turbulence. The flow over baffles has different fluid flow and heat transfer characteristics. The presence of these baffles causes the flow to separate, reattach and create reverse flow. If the baffles are staggered, they will cause the flow to deflect and impinge upon the opposite walls, increasing the washing action. Recently many investigations have been focused on the baffle-walled channel heat exchangers. Most studies discussed the optimal baffle geometry that enhance heat transfer performance for a given pumping power or flow rate. In the experimental efforts, Founti and Whitelaw [1] used LDA to deduce the velocity field in an axisymmetric heat exchanger with baffles on the shell-side surface. The similar distributions of the mean-flow velocity and turbulent intensity were found after two sets of baffles from the channel entrance. Later Berner et al. [2] and Berner et al. [3] obtained experimental results of mean velocity and turbulence distributions in flow around segmented baffles. Experimental investigation of characteristics of the turbulent flow and heat transfer inside the periodic cell formed between

* Corresponding author. Tel.: +886-6-275-7575x62172; fax: +886-6-235-2973.

E-mail address: ytyang@mail.ncku.edu.tw (Y.-T. Yang).

0017-9310/03/$ - see front matter
PII: S0017-9310(02)00360-5

Nomenclature

c_1, c_2	turbulent constant
C	inertia factor
d_p	particle diameter
D_h	hydraulic diameter
f	friction factor
H	channel height
h	baffle height
I	turbulence intensity
k_d	stagnant conductivity
k_e	effective thermal conductivity of the porous baffle
k_f	thermal conductivity of the fluid
k_t	thermal dispersion conductivity
K_p	permeability
k	turbulent kinetic energy
$\overline{Nu}$	averaged Nusselt number for baffled channel flow
$\overline{Nu}_s$	averaged Nusselt number for the smooth channel
P	pressure
Re	Reynolds number
S	baffle spacing
S_ϕ	source term
T	temperature
T_{in}	inlet temperature
U_{in}	inlet velocity
u	velocity in the x-direction
v	velocity in the y-direction

Greek symbols

ϕ	transported scalar
ρ	density
μ_ℓ, μ_t, μ_e	laminar, turbulent and effective viscosity
σ_k, σ_ε, σ_T	k–ε turbulence model constant for k, ε and T
v	porosity
α_p	thermal diffusivity of porous media
ε	turbulent energy dissipation rate

Subscripts

f	external flow field
p	porous media

segmented baffles staggered in a rectangular duct was studied by Habib et al. [4]. The experimental results indicated that the pressure loss increased as the baffle height did. For a given flow rate, local and average heat transfer parameters increase with increasing Reynolds number and baffle height. Numerical predictions of the flow and heat transfer in channels with staggered fins were investigated by Webb and Ramadhyani [5], Kelkar and Patankar [6], and Habib et al. [7]. Corrugated walls with or without fins may be used as passages in heat exchangers for the purpose of heat transfer augmentation presented by Amano et al. [8]. Most of the numerical research involving obstructions has been limited to two-dimensional cases. The hydraulic and thermal effects of placing normal baffles inside a three-dimensional channel were studied numerically by Lopez et al. [9]. A numerical investigation of laminar forced convective heat transfer was performed in a three-dimensional channel with baffles in which a uniform heat flux was applied to the top and bottom walls, and the sidewalls were considered adiabatic. They presented that three-dimensional effects on the friction factor of a channel with unity aspect ratio and a blockage ratio of 0.5 increased with an increase in Re.

From a literature search, it appears that the segmented baffles employed in all of the previous investigations are all solids. The experimental work of the porous-type baffles on the fluid flow and heat transfer in a rectangular channel was presented by Hwang [10]. The heat transfer and transport phenomena in the porous media which is an important process in many practical applications, e.g. heat exchanger, the pack-sphere bed, electronic cooling, chemical catalytic reactors, heat pipe technology etc. Porous media have large contact surface with fluids which enhance heat transfer performance. This topic was studied by many investigators [11–16]. Recently many studies have been focused on the interfacial problem of the fluid–porous media composite system [17]. The interfacial problems between the fluid–porous media are very complicated. Vafai and Thiyagaraja [18] considered the interface between porous media and external fluid field, and the interface between porous media and a solid boundary. Vafai and Kim [19] derived an exact solution which was studied by Beavers and Joseph [17]. In addition, Vafai and Kim [20] also found that the enhancement of thermal performance of the porous media mainly depend on the ratio of the effective thermal conductivity of the porous media to fluid thermal conductivity. The heat transfer of a flat plate mounted with porous block array was presented by Huang and Vafai [21]. They found that the porous block array significantly reduced the heat transfer rate on the flat plate. But the different trends were presented by Hadim [22]. Huang and Vafai [23] considered a forced convection problem in an isothermal parallel plate channel with porous block using a vorticity stream

function formulation. They found that significant heat transfer augmentation can be achieved through the use of multiple emplaced porous blocks. A numerical study of a porous block mounted on a heated wall in a laminar flow channel to enhance convection heat transfer rate was demonstrated by Fu et al. [24]. All the non-Darcian effects are considered. The results indicated that the thermal performances are enhanced by using a porous block with higher porosity and particle diameter.

Limited data exist for the case where the porous-type baffles are arranged on the top and bottom channel walls in a staggered manner and therefore as a preliminary to looking at a more realistic problem, numerical studies on effect of porous-type baffles are presented and compared with the only known experimental data of Hwang [10].

2. Mathematical formulation

A schematic diagram of forced convection enhancement in a channel using porous baffles is shown in Fig. 1. The fluid enters at T_{in} with a uniform velocity profile. The plate walls are maintained at constant T_{wall}. The flow is assumed to be steady, incompressible and two-dimensional. In addition, the thermophysical properties of the fluid and the porous matrix are assumed to be constant, and the porous medium is considered homogeneous, isotropic, nondeformable, and in local thermodynamic equilibrium with the fluid. In this study, the non-Darcy model is used to demonstrate the flow inside the porous region.

The governing equations to be considered are the time-averaged continuity, momentum, and energy equations. An eddy viscosity model is used to account for the effect of turbulence phenomena. Then, the governing equations can be written in the common form as

$$\frac{\partial}{\partial x}(\rho u\phi)+\frac{\partial}{\partial y}(\rho v\phi)=\frac{\partial}{\partial x}\left[\Gamma_\phi\frac{\partial\phi}{\partial x}\right]+\frac{\partial}{\partial y}\left[\Gamma_\phi\frac{\partial\phi}{\partial y}\right]+S_\phi, \tag{1}$$

where ϕ stands for the dependent variables u, v, k, T and ε; u, v are local time-averaged velocity in x and y directions respectively; Γ_ϕ and S_ϕ are the corresponding turbulent diffusion coefficient and source term respectively for general variable ϕ. The equations of the main flow region and the porous-baffle region are summarized in Tables 1 and 2.

2.1. Boundary conditions

The computational domain boundaries are shown in Fig. 2. The boundary conditions for the above set of governing equations are

(1) Inlet boundary (A–B)

$$u=U_{in},\quad v=0,\quad k=k_{in}=IU_{in}^2,\quad T=T_{in},$$

$$\varepsilon=\frac{k_{in}^{3/2}}{\lambda D_h},$$

where I is the turbulence intensity, λ is the length scale constant and D_h is the hydraulic diameter.

(2) Wall boundary (A–D and B–C)

In the k–ε model, the near-wall region was simulated by a two zone model, i.e. viscous sublayer and fully turbulent zone, and the wall function suggested by Launder and Spalding [25] was used.

(3) Exit boundary (C–D)

A zero gradient condition except the velocity component v is employed across the outlet boundary. Although this boundary condition is strictly valid only when flow is fully developed, it is also permissible for sufficient downstream from the region of interest.

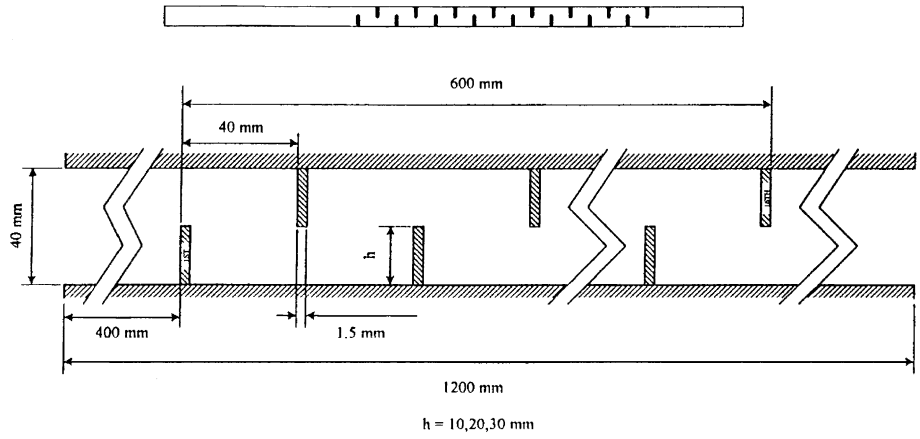

Fig. 1. Physical coordinate system.

Table 1
Summary of equations solved for the main flow region

Equations	ϕ	Γ_ϕ	S_ϕ
Continuity	1	0	0
x-momentum	u	μ_e	$-\frac{\partial p}{\partial x}+\frac{\partial}{\partial x}\left[\mu_e\frac{\partial u}{\partial x}\right]+\frac{\partial}{\partial y}\left[\mu_e\frac{\partial v}{\partial x}\right]$
y-momentum	v	μ_e	$-\frac{\partial p}{\partial y}+\frac{\partial}{\partial x}\left[\mu_e\frac{\partial u}{\partial y}\right]+\frac{\partial}{\partial y}\left[\mu_e\frac{\partial v}{\partial y}\right]$
Energy	T	$\frac{\mu_e}{\sigma_T}$	0
Turbulent energy	k	$\mu_\ell+\frac{\mu_t}{\sigma_k}$	$-\rho\varepsilon+G$
Turbulent dissipation	ε	$\mu_\ell+\frac{\mu_t}{\sigma_\varepsilon}$	$\frac{\varepsilon}{k}(c_1G-c_2\rho\varepsilon)$

$G=\mu_t\left\{2\left[\left(\frac{\partial u}{\partial x}\right)^2+\left(\frac{\partial v}{\partial y}\right)^2\right]+\left[\frac{\partial u}{\partial y}+\frac{\partial v}{\partial x}\right]^2\right\}$.
$\mu_e=\mu_\ell+\mu_t$.

Table 2
Summary of equations solved for the porous-baffle region

Equations	ϕ	Γ_ϕ	S_ϕ
Continuity	1	0	0
x-momentum	u	μ_ℓ	$-v^2\frac{\partial p}{\partial x}+(v-1)\mu_\ell\left[\frac{\partial^2 u}{\partial^2 x^2}+\frac{\partial^2 u}{\partial^2 y^2}\right]$ $-\rho v^2 uv\frac{\partial}{\partial y}\left[\frac{1}{v}\right]-\frac{\mu_\ell}{K_p}v^2u-\rho C\lvert U\rvert v^2u$
y-momentum	v	μ_ℓ	$-v^2\frac{\partial p}{\partial y}+(v-1)\mu_\ell\left[\frac{\partial^2 v}{\partial^2 x^2}+\frac{\partial^2 v}{\partial^2 y^2}\right]$ $-\rho v^2 vv\frac{\partial}{\partial y}\left[\frac{1}{v}\right]-\frac{\mu_\ell}{K_p}v^2v-\rho C\lvert U\rvert v^2v$
Energy	T	α_p/ρ	0

$K_p=\frac{d_p^2v^3}{150(1-v)^2}$; $C=\frac{1.75}{\sqrt{150}v^{1.5}}$; $|U|=\sqrt{u^2+v^2}$.

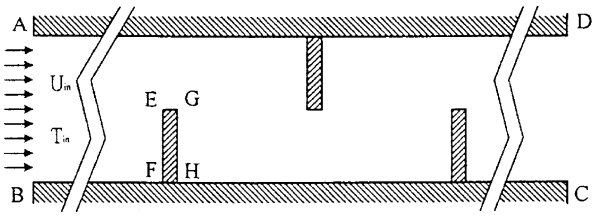

Fig. 2. Boundary conditions.

(4) Interfacial boundary (E–F, E–G and G–H)

At the porous/fluid interface, the following quantities evaluated in both the porous and fluid regions are matched.

On surface E–F and G–H

$u_f=u_p,\quad v_f=v_p,\quad p_f=p_p,$

$\frac{\partial u_f}{\partial x}=\frac{\partial u_p}{\partial x},\quad \frac{\partial v_f}{\partial x}=\frac{\partial v_p}{\partial x},$

$T_f=T_p,\quad k_f\frac{\partial T_f}{\partial x}=k_e\frac{\partial T_p}{\partial x},$

where $k_e=k_d+k_t$ given by Fu et al. [24]

$k=\frac{\partial\varepsilon}{\partial x}=0.$

On surface E–G

$u_f=u_p,\quad v_f=v_p,\quad p_f=p_p,$

$\frac{\partial u_f}{\partial y}=\frac{\partial u_p}{\partial y},\quad \frac{\partial v_f}{\partial y}=\frac{\partial v_p}{\partial y},$

$$T_f = T_p, \quad k_f \frac{\partial T_f}{\partial y} = k_e \frac{\partial T_p}{\partial y},$$

$$k = \frac{\partial \varepsilon}{\partial y} = 0.$$

3. Numerical procedure

In this study, the computational domain was chosen to be larger than the physical domain to eliminate the entrance and exit effects and to satisfy continuity at the exit. A nonuniform grid system with a large concentration of nodes in regions of steep gradients, such as those close to the walls and porous baffles was employed. The numerical method used in the present study is based on the SIMPLEST algorithm of Patankar [26]. The conservation equations are discretized by control volume based finite difference method with power-law scheme. The set of difference equations are solved iteratively using a line by line solution method in conjunction with a tridiagonal matrix form. The solution is considered to be converged when the normalized residual of the algebraic equation is less than a prescribed value of 10^{-4}. The comparison of the streamwise mean-velocity along the axial direction for the porous-type baffles ($v = 0.42$) is shown in Fig. 3. Based on the grid independent study, the grid (831×66) was used for the numerical calculations. These computations performed on a PC Pentium 200 MMX, total iterations for each case were 3000–5000, depending upon the different governing parameters, taken about 15–30 h CPU time.

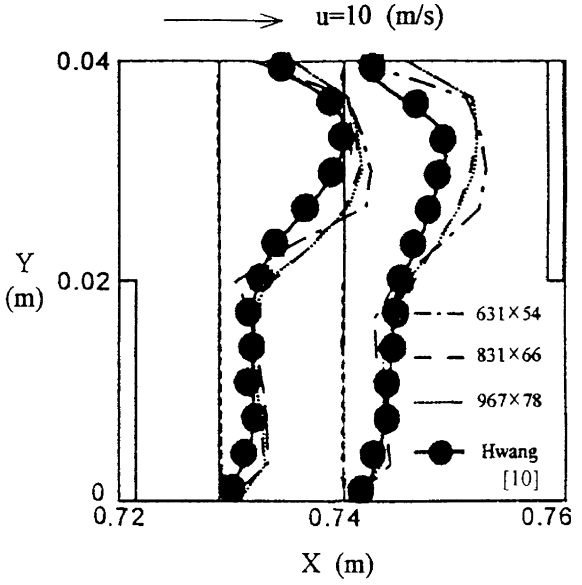

Fig. 3. Effect of grid refinement on streamwise velocity.

4. Results and discussion

From the flowfield measurements in the previous works of Founti and Whitelaw [1] and Berner et al. [2], it has been presented that the hydraulic periodicity of the airflow was achieved in the region after the flow passed over baffles. According to the experimental work of Hwang [10], the periodically fully developed heat transfer and fluid flow data were taken between the 9th and 11th baffles.

4.1. Velocity vector plots

Fig. 4(a) and (b) shows the velocity vector plots for solid-type baffled at $Re = 5 \times 10^4$, $h/H = 0.25$ and 0.5. The flow is a turbulent shear flow when over the solid-type baffles. It indicates that the common features are

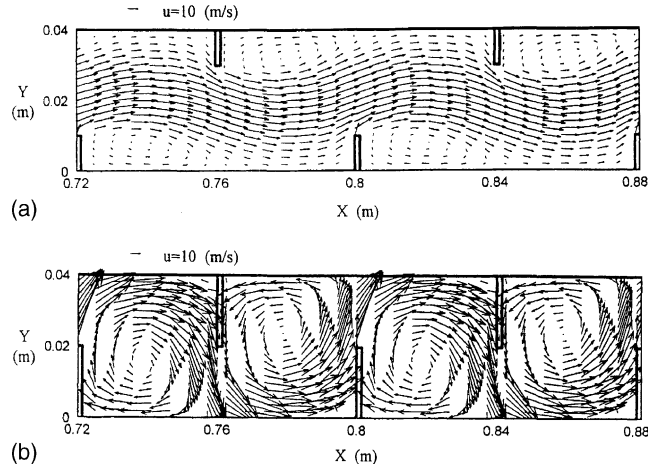

Fig. 4. Velocity vectors for solid-type baffles for $Re = 5 \times 10^4$: (a) $h/H = 0.25$ and (b) $h/H = 0.5$.

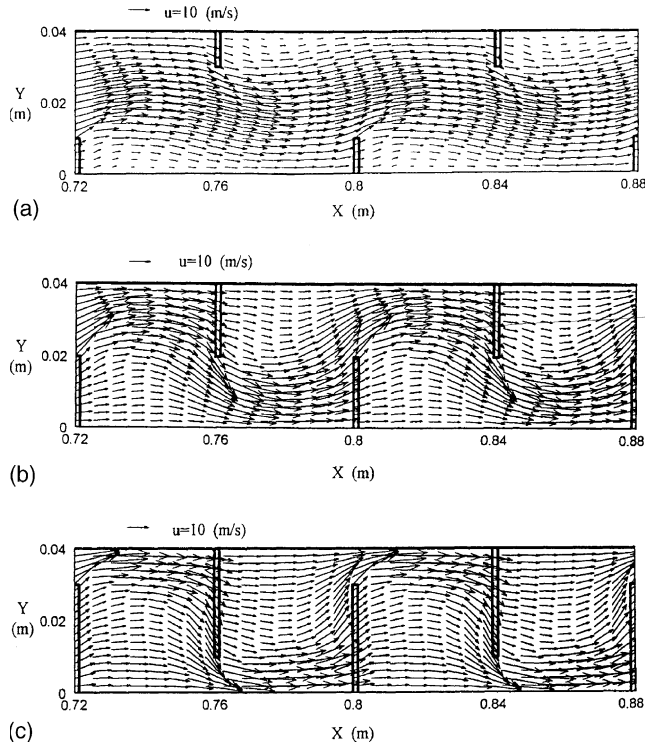

Fig. 5. Velocity vectors for porous-type baffles for $v = 0.42$, $Re = 5 \times 10^4$: (a) $h/H = 0.25$, (b) $h/H = 0.5$ and (c) $h/H = 0.75$.

the core flow regions and the recirculation regions when flow is over the solid-type baffle, the fluid turning from the upstream bottom channel wall into the contraction produces a strong shear layer from the baffle tip attaching the bottom wall, which forms a large recirculation bubble behind the baffle. The zigzag motion means flow across the staggered baffles in the channel will impinge on the top and bottom channel walls. As the blockage ratio increases, the core flow region becomes smaller. The result indicates that the impingement area is reduced and the central recirculating region changes its orientation. Fig. 5(a)–(c) shows the flow patterns as for flow over the porous-type baffles. From the numerical calculations of the flow field, it indicates that the flow patterns around the solid- and porous-type baffles are entirely different due to different transport phenomena. The recirculation bubble that existed behind the solid-type baffle disappears in the corresponding region of the porous-type baffle. When flow is over the porous-type baffles, some of the fluid passes through the porous medium and the remainder goes around the baffles. The flow structures between the lower and upper half parts are significantly different for this porous-type channel case. As for the porous-type baffles, the flow decelerates before entering the upper half part of the porous-type baffles, and accelerates as it passes through the full opening between the lower half part of the baffles and the channel walls.

4.2. Effect of porosity

The effect of the porosity is shown in Fig. 6(a)–(d) for $Re = 3 \times 10^4$, $h/H = 0.5$. As for the flow over the solid-type baffle ($v = 0$), the flow is deflected due to the presence of the baffles and impinges on the top and bottom walls. When the flow is over the porous-type baffles, the flow partly passes through the baffle and directly impinges the recirculation cell, and hence breaks up the recirculating bubble. The results indicate that the transport phenomena have been greatly improved by using the porous-type baffle instead of the solid-type baffles on the channel wall. For the higher porosity, the less cross-sectional blockage is accompanied which largely reduces the form drag of the porous-baffled channel.

4.3. Effect of Reynolds number

The effects of Re on the flow field of high porosity $v = 0.7$ and $h/H = 0.5$ are shown in Fig. 7(a)–(c). The features of the plots are Reynolds number dependence. The recirculation bubble disappears behind the porous-type baffle.

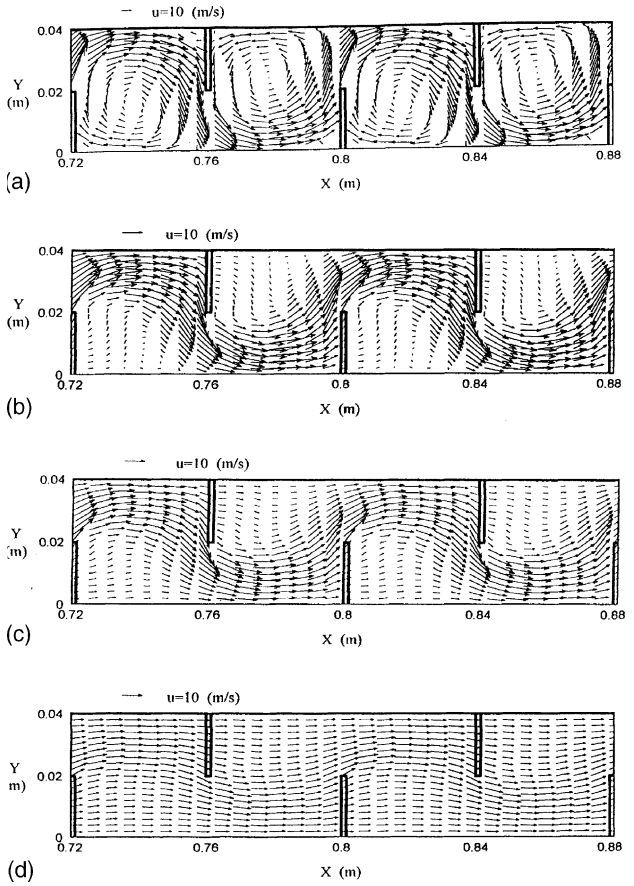

Fig. 6. Porosity effects on velocity vectors for $h/H = 0.5$, $Re = 3 \times 10^4$: (a) $v = 0$, (b) $v = 0.2$, (c) $v = 0.42$ and (d) $v = 0.7$.

4.4. Effect of blockage ratio

The effect of blockage ratio (h/H) on the friction factor for the solid-type baffles is shown in Fig. 8. The results indicate that the friction factor increases with increasing h/H because the cross-sectional area where the flow passes through gets smaller for a fixed baffle spacing and a given Reynolds number. It is further found that at the same baffle height $h/H = 0.5$ the friction factor of predictions and results of Hwang [10] is nearly the same for the solid-type baffles. For the higher baffles, $h/H = 0.5$ and 0.75, the friction is nearly independent of the Reynolds number.

4.5. Effect of heat transfer

The heat transfer coefficient is presented here in terms of the ratio of centerline-averaged Nusselt number for the solid baffle duct to those for the smooth one, $\overline{Nu}/\overline{Nu}_s$, where $\overline{Nu}_s$ is the value of averaged Nusselt number for the smooth channel. As shown in Fig. 9, it can be seen that as the blockage ratio increases, the effect of Reynolds number becomes more pronounced for the solid-type-baffled walls. As for the effect of blockage ratio on the heat transfer, the Nusselt number ratio increases as the baffle height is increased because of the augmentation of the flow acceleration caused by increasing the cross-sectional blockage of the channel. It is further found that at the same baffle height $h/H = 0.5$ the predictions of the average heat transfer ratio is higher than that of the experimental results of Hwang [10] in this solid-type-baffled cases.

5. Conclusions

The numerical calculations compared with the experimental data of Hwang [10] are presented for turbulent flow and heat transfer in a rectangular channel with segmented solid-type and porous-type baffles that are staggeringly arranged on the top and bottom wall of the channel. The results are presented for a fixed baffle spacing ($S/H = 1.0$) and different values of Reynolds number ($1 \times 10^4 \leqslant Re \leqslant 5 \times 10^4$), baffle heights

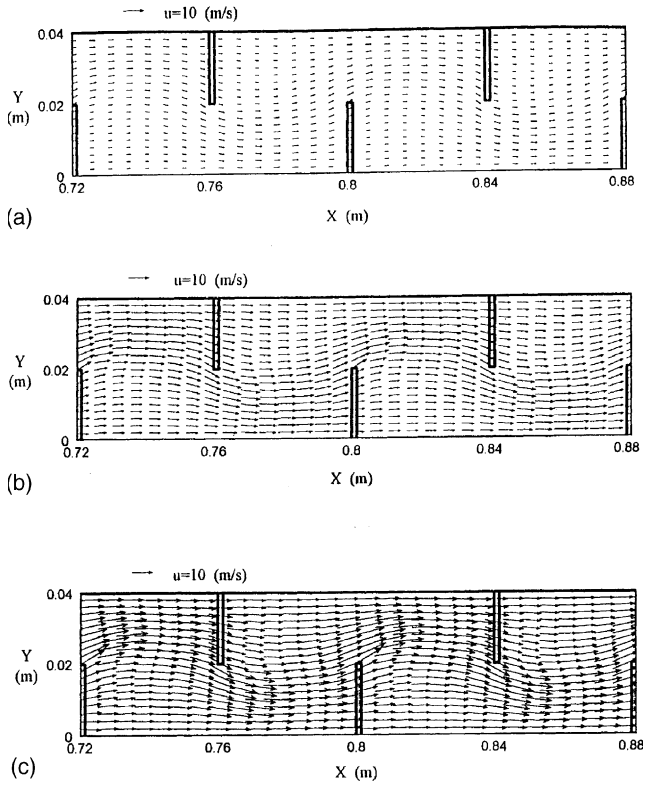

Fig. 7. Reynolds number effects on velocity field of high porosity for $v = 0.7$, $h/H = 0.5$: (a) $Re = 1 \times 10^4$, (b) $Re = 3 \times 10^4$ and (c) $Re = 5 \times 10^4$.

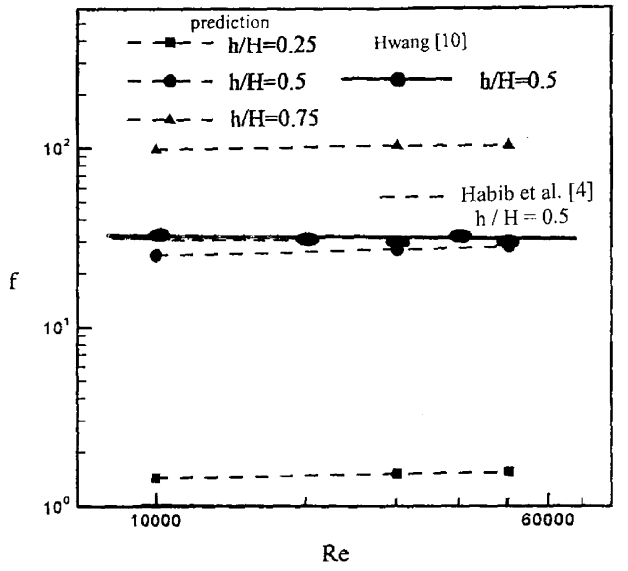

Fig. 8. Blockage ratio effects on the friction factor for the solid-type baffles.

($h/H = 0.25$, 0.5 and 0.75) and different porosities ($v =$ 0.2, 0.42 and 0.7). Conclusions can be summarized as follows:

(1) There are three effects present when the solid-type baffles are replaced by the porous-type baffles, reducing the effective thermal conductivity of the baf-

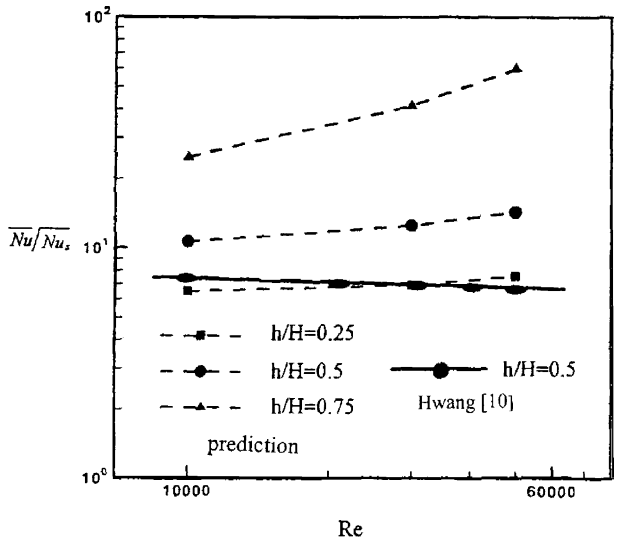

Fig. 9. Blockage ratio effects on centerline-averaged Nusselt number for solid-type baffles.

fle, increasing of heat transfer surface and changing the flow transport phenomena.

(2) The flow field numerical calculations present that the different transport phenomena around the solid-type and porous-type baffles exist behind the baffles.

(3) The porous-type baffle channel has a lower friction factor relative to the solid-type baffle channel due to less channel blockage.

(4) At the higher baffle height, the level of heat transfer augmentation is nearly the same for the porous-type baffle, the only difference being the Reynolds number dependence expected.

(5) Certain discrepancies between calculations and the available data of Hwang [10] may be caused by the isotropic assumption, modification of the porous media or uncertainty of the measurements.

Acknowledgements

We would like to thank the National Science Council of the Republic of China for supporting this work under contract no. NSC 88-2212-E-006-031.

References

[1] M.A. Founti, J.H. Whitelaw, Shell side flow in a model-disc and doughnut heat exchanger, Tech. Report FS/81/37, Mech. Eng. Dept., Imperial College, London, UK, 1981.

[2] C. Berner, F. Durst, D.M. McEligot, Flow around baffles, Trans. ASME J. Heat Transfer 106 (1984) 743–749.

[3] C. Berner, F. Durst, D.M. McEligot, Streamwise-periodic flow around baffles, in: Proceedings of the 2nd International Conference on Applications of Laser Anemometry to Fluid Mechanics, Lisbon, Portugal, 1984.

[4] M.A. Habib, A.M. Mobarak, M.A. Sallak, E.A. Abdel Hadi, R.I. Affify, Experimental investigation of heat transfer and flow over baffles of different heights, Trans. ASME J. Heat Transfer 116 (1994) 363–368.

[5] B.W. Webb, S. Ramadhyani, Conjugate heat transfer in a channel with staggered ribs, Int. J. Heat Mass Transfer 28 (1985) 1679–1687.

[6] K.M. Kelkar, S.V. Patankar, Numerical prediction of flow and heat transfer in parallel plate channel with staggered fins, Trans. ASME J. Heat Transfer 109 (1987) 25–30.

[7] M.A. Habib, A.E. Attya, D.M. McEligot, Calculation of turbulent flow and heat transfer in channels with streamwise-periodic flow, Trans. ASME J. Turbomach. 110 (1988) 405–411.

[8] R.S. Amano, A. Bagherle, R.J. Smith, T.G. Niess, Turbulent heat transfer in corrugated wall channels with and without fins, Trans. ASME J. Heat Transfer 109 (1987) 62–67.

[9] J.R. Lopez, N.K. Anand, L.S. Fletcher, Heat transfer in a three-dimensional channel with baffles, Numer. Heat Transfer A 30 (1996) 189–205.

[10] J.J. Hwang, Turbulent heat transfer and fluid flow in a porous-baffled channel, AIAA J. Thermophys. Heat Transfer 11 (1997) 429–436.

[11] K. Vafai, C.L. Tien, Boundary and inertia effects on flow and heat transfer in porous media, Int. J. Heat Mass Transfer 24 (1981) 195–203.

[12] M. Kaviany, Laminar flow through a porous channel bounded by isothermal parallel plates, Int. J. Heat Mass Transfer 28 (1985) 851–858.

[13] R.F. Benenati, C.B. Brosilow, Void fraction distribution in a bed of spheres, AIChE J. 8 (1962) 359–361.

[14] K. Vafai, Convection flow and heat transfer in variable porous media, J. Fluid Mech. 147 (1984) 233–259.
[15] K. Vafai, R.L. Alkire, C.L. Tien, An experimental investigation of heat transfer in variable porosity media, Trans. ASME J. Heat Transfer 107 (1985) 642–647.
[16] P. Cheng, C.T. Hsu, Fully developed forced convective flow through an annular packed-sphere bed with wall effects, Int. J. Heat Mass Transfer 29 (1986) 1843–1853.
[17] G.S. Beavers, D.D. Joseph, Boundary condition at a naturally permeable wall, J. Fluid Mech. 30 (1967) 197–207.
[18] K. Vafai, R. Thiyagaraja, Analysis of flow and heat transfer at the interface region of a porous medium, Int. J. Heat Mass Transfer 30 (1987) 1391–1405.
[19] K. Vafai, S.J. Kim, Fluid mechanics of the interface region between a porous medium and a fluid layer—an exact solution, Int. J. Heat Fluid Flow 11 (1990) 254–256.
[20] K. Vafai, S.J. Kim, Analysis of surface enhancement by a porous substrate, Trans. ASME. J. Heat Transfer 112 (1990) 700–706.
[21] P.C. Huang, K. Vafai, Flow and heat transfer control over an external surface using a porous block array arrangement, Int. J. Heat Mass Transfer 36 (1993) 4019–4032.
[22] A. Hadim, Forced convection in a porous channel with localized heat source, Trans. ASME J. Heat Transfer 116 (1994) 465–472.
[23] P.C. Huang, K. Vafai, Analysis of forced convection enhancement in a channel using porous blacks, AIAA J. Thermophys. Heat Transfer 8 (1994) 563–573.
[24] W.S. Fu, H.C. Huang, W.Y. Liou, Thermal enhancement in laminar channel flow with a porous block, Int. J. Heat Mass Transfer 39 (1996) 2165–2175.
[25] B.E. Launder, D.B. Spalding, The numerical computation of turbulent flow, Comput. Meth. Appl. Mech. Eng. 3 (1974) 269–289.
[26] S.V. Patankar, Numerical Heat Transfer and Fluid Flow, McGraw-Hill, New York, 1980.